High Frequency Atomic Magnetometer by Use of Electromagnetically Induced Transparency

G. Katsoprinakis,[1,2] D. Petrosyan,[2] and I. K. Kominis[1,2,*]

[1]*Department of Physics, University of Crete, Heraklion 71103, Greece*

[2]*Institute of Electronic Structure & Laser, Foundation for Research and Technology, Heraklion 71110, Greece*

(Received 7 March 2006; published 6 December 2006)

Atomic magnetometers have achieved magnetic sensitivities in the subfemtotesla regime. Their bandwidth is determined by the transverse spin relaxation rate, $1/T_2$, which also determines the magnetic sensitivity. It is theoretically demonstrated that by using an electromagnetically induced transparent probe beam in a pump-probe atomic magnetometer, it is possible to operate the latter at frequencies much higher than its bandwidth, maintaining a high signal-to-noise ratio.

DOI: 10.1103/PhysRevLett.97.230801 PACS numbers: 07.55.Ge, 32.80.Bx, 42.50.Gy

Atomic magnetometers [1–3] have recently become competitive with the well-established superconducting sensors (SQUIDs) [4], reaching magnetic field sensitivities on the order of 1 $\mathrm{fT}/\sqrt{\mathrm{Hz}}$. In particular, the spin-exchange relaxation-free magnetometer [5,6] has demonstrated a sensitivity of 0.54 $\mathrm{fT}/\sqrt{\mathrm{Hz}}$ and has a projected shot-noise limited sensitivity of less than 0.01 $\mathrm{fT}/\sqrt{\mathrm{Hz}}$ with a measurement volume less than 1 cm^3. These sensitivity levels enable several applications of atomic magnetometers, ranging from biomagnetic measurements [7] to precision tests of fundamental symmetries [8]. For almost all of the magnetometer's applications, the frequency response is of equal importance. The zero-field pump-probe magnetometer discussed in [6] has a frequency response equivalent to a first order low-pass filter with a cutoff frequency ω_c on the order of $1/T_2$, where $1/T_2$ is the alkali atom transverse spin relaxation rate, proportional to the atom density. To increase the bandwidth it is therefore necessary to operate the magnetometer in the optically very thick regime, necessitating impractically high temperatures and degrading optical pumping. In this Letter we show theoretically that by creating electromagnetically induced transparency (EIT) of the probe beam, we can operate the magnetometer closer to the atomic resonance. The enhancement of the magnetometer's response thus obtained allows its operation at frequencies well beyond the bandwidth, while maintaining a high signal-to-noise ratio.

We will first consider an optical pumping pump-probe magnetometer with two-level (spin 1/2) ground and excited state atoms (TLA). In Fig. 1(a) we display the geometry of the optical pumping magnetometer. The atoms are optically pumped along the $\hat{\mathbf{z}}$ direction with a circularly polarized pump laser, producing a spin polarization, P_z, of the atomic vapor. A magnetic field along the $\hat{\mathbf{y}}$ axis, B_y, produces a polarization component P_x, proportional to B_y, which induces a rotation of the polarization plane of a linearly $\hat{\mathbf{y}}$-polarized probe beam, that illuminates the vapor along the $\hat{\mathbf{x}}$ axis. This is due to the paramagnetic Faraday effect. The rotation angle, ϕ, is proportional to P_x, and thus to B_y. The measurement of ϕ is based on the detection of the probe laser intensity falling on a photodetector after a crossed analyzer. The measured signal is

$$S = I_0 2\phi e^{-N\sigma/A}, \tag{1}$$

where I_0 is the incident probe laser intensity, σ is the probe laser absorption cross section, A is the probe laser beam area, and N the number of alkali atoms in the vapor volume, $V = A\ell$, traversed by the probe laser. The Bloch equations describing the time evolution of the polarization are

$$\frac{d\mathbf{P}}{dt} = \gamma\mathbf{P}\times\mathbf{B} - (R + R_{\mathrm{pr}} + 1/T_2)\mathbf{P} + R\hat{\mathbf{z}}, \tag{2}$$

where R is the optical pumping rate along $\hat{\mathbf{z}}$ and R_{pr} is the pumping rate due to the probe beam. Both add to the ground-state spin decoherence. If we only consider an ac-magnetic field along the $\hat{\mathbf{y}}$ direction with frequency ω, then the solution of the above equations in the rotating frame (taking into account that $\gamma B_y \ll 1/T_2$) is

$$P_x = \frac{\gamma B_y P_z}{\sqrt{\omega^2 + \omega_c^2}}, \tag{3}$$

where $\omega_c = R + R_{\mathrm{pr}} + 1/T_2$ is the magnetometer's bandwidth and $P_z = R/\omega_c$. If we define $J_x = \sum_{i=1}^{N} J_x^{(i)}$ as the $\hat{\mathbf{x}}$

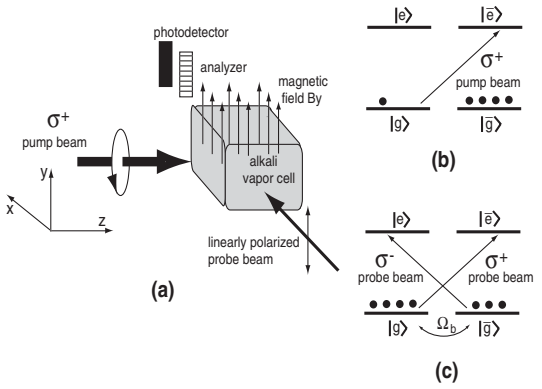

FIG. 1. Optical Pumping Pump-Probe Magnetometer. (a) Experimental scheme. (b) Optical pumping viewed along the $\hat{\mathbf{z}}$ quantization axis. (c) Probing viewed along the $\hat{\mathbf{x}}$ quantization axis.

component of the total spin of the N-atom ensemble, we can write $\langle J_x\rangle = NP_x$. The measured Faraday rotation angle is proportional to $\langle J_x\rangle$, namely

$$\phi \equiv \langle\phi\rangle = \frac{\delta}{\Gamma}\frac{\sigma}{A}\langle J_x\rangle \equiv \kappa\langle J_x\rangle, \tag{4}$$

where δ is the probe laser detuning and Γ the FWHM of the optical transition. In the following we will show that by using EIT we can enhance the rotation angle ϕ for a given magnetic field B_y by a factor β_ϕ, where $\beta_\phi = 1$ in the usual (no EIT) case. The uncertainty in the measured magnetic field is

$$\Delta B_y = \frac{\Delta\phi}{|\partial\langle\phi\rangle/\partial B_y|}, \tag{5}$$

where $\Delta\phi \equiv \sqrt{\langle\phi^2\rangle - \langle\phi\rangle^2}$. In order to maximize the magnetic sensitivity and the measured signal, the derivative $\partial\langle\phi\rangle/\partial B_y$ and P_z have to be maximum. It easily follows that both conditions are met when $R_{\rm pr} \lesssim R \approx 1/T_2$. Ignoring factors on the order of unity we find that $\partial\langle\phi\rangle/\partial B_y = \beta_\phi\kappa\gamma T_2\langle J_z\rangle$, where $\langle J_z\rangle/N = P_z$ is the spin polarization produced along the $\hat{\mathbf{z}}$ axis by optical pumping, and the magnetometer's bandwidth is $\omega_c = 1/T_2$. For high frequencies $\omega \gg \omega_c$, it follows that

$$\left.\frac{\partial\langle\phi\rangle}{\partial B_y}\right|_{\omega\gg\omega_c} = \frac{\omega_c}{\omega}\left.\frac{\partial\langle\varphi\rangle}{\partial B_y}\right|_{\omega\ll\omega_c}. \tag{6}$$

The uncertainty in the rotation angle measurement has two sources: spin noise and probe laser shot noise. Therefore, $\Delta\phi = \sqrt{\Delta\phi^2_{\rm spins} + \Delta\phi^2_{\rm laser}}$, with $\Delta\phi_{\rm spins} = \beta_\phi\kappa\Delta J_x$, and hence $\Delta B_y = \sqrt{\Delta B^2_{y,\rm spins} + \Delta B^2_{y,\rm laser}}$, where

$$\Delta B_{y,\rm spins} = \frac{1}{\gamma T_2}\frac{\Delta J_x}{\langle J_z\rangle}, \qquad \Delta B_{y,\rm laser} = \frac{1}{\gamma T_2}\frac{\Delta\phi_{\rm laser}}{\beta_\phi\kappa\langle J_z\rangle}. \tag{7}$$

Since spin noise is band limited to $\omega_c = 1/T_2$, the power spectral density of the magnetic field noise, $\delta B^2_{y,\rm spins}$ (in units of T^2/Hz), will be given by $\Delta B^2_{y,\rm spins} = \frac{1}{T_2}\delta B^2_{y,\rm spins}$. The uncertainty in the rotation angle, $\Delta\phi_{\rm laser}$, due to the shot-noise fluctuations of the probe laser intensity detected after transmission through the vapor, is [9] $\Delta\phi_{\rm laser} = 1/\sqrt{2\epsilon\dot{N}_{\rm tr}}$, where $\dot{N}_{\rm tr}$ is the transmitted photon flux and ϵ the photon detection quantum efficiency. The magnetic sensitivity can thus be written, after introducing the spin-squeezing parameter [10] $\xi = \sqrt{N}\Delta J_x/\langle J_z\rangle$, as

$$\delta B_y = \frac{1}{\gamma\sqrt{NT_2}}\sqrt{\xi^2 + \frac{\eta^2}{\beta^2_\phi}}, \tag{8}$$

where, after setting $\dot{N}_{\rm tr} = P_{\rm inc}e^{-N\sigma/A}/(hc/\lambda)$ with $P_{\rm inc}$ being the incident probe laser power,

$$\eta^2 = \frac{(hc/\lambda)Ne^{N\sigma/A}}{\epsilon P_{\rm inc}T_2(\kappa\langle J_z\rangle)^2}. \tag{9}$$

Thus the spin-noise term in the magnetic sensitivity is unaffected by an enhanced rotation angle, whereas the photon noise is suppressed. Usually the latter can be neglected, i.e., $\eta^2 \ll 1$. Moreover, without spin-squeezed atomic ensembles, $\xi = 1$, so that $\delta B = 1/\gamma\sqrt{NT_2}$, which is the formula most frequently used, and which is at the level of 0.01 $\mathrm{fT}/\sqrt{\mathrm{Hz}}$ for the operating parameters of the spin-exchange relaxation-free magnetometer. In actual experiments there are other dominant noise sources limiting the sensitivity to values higher than the shot-noise sensitivity we just calculated. The most common is thermal magnetic noise arising from Johnson currents in the conductive magnetic shields, which is on the order of 1–10 $\mathrm{fT}/\sqrt{\mathrm{Hz}}$, well above the magnetometer's shot noise. Considering [11] that the thermal magnetic noise is band limited to about 1 kHz, the total noise, N, in the measured signal (1), will be for high frequencies $\omega \gg \omega_c$, to within an arbitrary factor,

$$N = \sqrt{\left(\frac{\omega_c}{\omega}\beta_\phi\right)^2\delta\phi^2_{\rm thermal} + \delta\phi^2_{\rm nm}}, \tag{10}$$

where $\delta\phi_{\rm thermal}$ is the low frequency ($\omega \ll \omega_c$) rotation angle fluctuation due to the thermal magnetic field and $\delta\phi_{\rm nm}$ represents all other noise sources of nonmagnetic origin. Applying a magnetic field at frequency ω, corresponding to a rotation angle ϕ, the signal will be

$$S_{\omega\gg\omega_c}(\beta_\phi) = \left(\frac{\omega_c}{\omega}\beta_\phi\right)S_{\omega\ll\omega_c}(\beta_\phi = 1). \tag{11}$$

There are at least two ways of taking advantage of the enhancement β_ϕ. First, one can choose $\omega > \omega_c$ so that $(\frac{\omega_c}{\omega}\beta_\phi)\delta\phi_{\rm thermal} \gg \delta\phi_{\rm nm}$. This way we can suppress all nonmagnetic noise sources while operating at a high frequency and keeping $\frac{S}{N}(\beta_\phi)_{\omega\gg\omega_c} \gtrsim \frac{S}{N}(\beta_\phi = 1)_{\omega\ll\omega_c}$. For example, for $\beta_\phi \approx 100$ and a bandwidth $\omega_c = 2\pi\times 20$ Hz, as reported in [6], we can choose $\omega = 50\omega_c = 2\pi\times 1$ kHz as an operating frequency. Second, one can approach shot-noise limited magnetic field detection, albeit at a lower magnetic sensitivity, by using a high relaxation rate atom, such as cesium (for which $\omega_c = 1/T_2 \approx 1$ kHz and $\delta B_y \approx 0.1$ $\mathrm{fT}/\sqrt{\mathrm{Hz}}$), in order to move into the frequency region of the falloff of the thermal magnetic noise (a few kHz), while enhancing (by β_ϕ) spin noise.

In order to create this rotation angle enhancement, we will consider the inclusion of two more ground-state sublevels (belonging to a different ground-state hyperfine level of a realistic alkali atom), and we will also add a strong drive, linearly polarized laser beam, copropagating with the weaker probe laser. Both drive and probe lasers can be decomposed into a σ^+ and a σ^- part, inducing the couplings shown in Fig. 2. We thus obtain two coupled Λ systems, allowing the probe laser to experience a steep dispersion near resonance. It is moreover possible to completely eliminate absorption by means of a small repumping rate from the probe-ground states to the drive ground

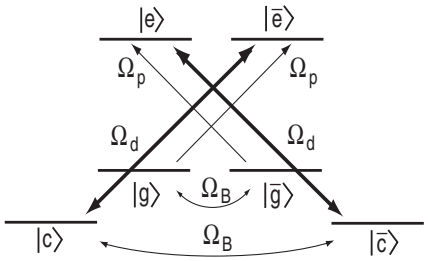

FIG. 2. Inclusion of ground-state sublevels $|c\rangle$, $|\bar{c}\rangle$, and of the drive laser, coupling them to $|\bar{e}\rangle$ and $|e\rangle$, respectively. The levels are degenerate since along the $\hat{\mathbf{x}}$ axis the magnetic field is zero.

states, thus creating a region of negative absorption (gain) and tuning the lasers so that zero-absorption coincides with large dispersion, as has been already demonstrated [12]. This incoherent repopulation of the drive states is achieved by the present optical pumping laser (which couples only to the $|g\rangle$, $|\bar{g}\rangle$ states). The dynamics of the system are governed by the Liouville equation:

$$i\hbar\frac{d\rho}{dt} = [\mathcal{H}, \rho] + \mathcal{R}(\rho), \tag{12}$$

where ρ is the 6×6 density matrix with elements ρ_{ij}, with $i, j = 1, \ldots, 6$ corresponding to the states $\bar{g}$, e, $\bar{c}$, g, $\bar{e}$, c, respectively. The Hamiltonian $\mathcal{H}$ contains the coherent interaction of the atoms with the probe laser, the drive laser, and the applied magnetic field, and is given by

$$\mathcal{H} = \hbar\begin{pmatrix} \delta_p & \Omega_p & 0 & -i\Omega_B & 0 & 0 \\ \Omega_p^* & 0 & \Omega_d^* & 0 & 0 & 0 \\ 0 & \Omega_d & \delta_d & 0 & 0 & -i\Omega_B \\ i\Omega_B & 0 & 0 & \delta_p & \Omega_p & 0 \\ 0 & 0 & 0 & \Omega_p^* & 0 & \Omega_d^* \\ 0 & 0 & i\Omega_B & 0 & \Omega_d & \delta_d \end{pmatrix}, \tag{13}$$

where Ω_p (Ω_d) and δ_p (δ_d) are the probe (drive) Rabi frequency and detuning, respectively, and $\Omega_B = \gamma B_y$ is the Larmor frequency. The relaxation matrix contains the usual decay of the coherences involving the excited state, as well as decay of the ground-state coherences with a rate of $1/T_2$, and the decay of the ground-state populations ρ_{ii}, where $i = g, \bar{g}, c, \bar{c}$, towards the thermal equilibrium value of $1/4$ at the same rate. Allowing only linear terms in the magnetic field, we get the ground-state populations:

$$\rho_{\substack{\bar{g}\,\bar{g}\\ g\,g}} \simeq \rho_{gg}^{(0)}(1 \pm \tfrac{1}{2}T_2\Omega_B) \tag{14}$$

and $\rho_{\bar{c}\,\bar{c}} \approx \rho_{cc} \approx \rho_{cc}^{(0)}$, where the zero magnetic field populations are given by $\rho_{\substack{gg\\ cc}}^{(0)} \simeq \frac{1}{4}(1 \pm \frac{1-s/2}{1+(5/2)s})$ with $s \approx \frac{\delta_d^2/\Omega_d^2}{T_2\Gamma}$. The coherences of the probe transitions, which define the linear susceptibility of the system, are

$$\rho_{\substack{\bar{g}e\\ g\bar{e}}} = \rho_{ge}^{(0)} \pm \rho_{ge}^{(B)} \tag{15}$$

$$\rho_{ge}^{(0)} \simeq \frac{\rho_{cc}^{(0)}\frac{\Omega_d^2}{D_{pd}} - \rho_{gg}^{(0)}D_d^*\left[1 - \frac{1/T_2}{4D_{pd}}\frac{\frac{\Omega_d^2}{D_{pd}} + \frac{D_p/T_2}{2D_{pd}}}{D_p + \Omega_d^2/D_{pd}}\right]}{D_d^*\left[(D_p + \Omega_d^2/D_{pd}) - \frac{(\frac{D_p/T_2}{2D_{pd}})^2}{D_p + \Omega_d^2/D_{pd}}\right]} i\Omega_p$$
$$\rho_{ge}^{(B)} \simeq \frac{1}{4}\left[\frac{\frac{1}{2} - \frac{1/T_2}{D_{pd}}\frac{\Omega_d^2/D_{pd}}{D_p + \Omega_d^2/D_{pd}}}{D_p + \Omega_d^2/D_{pd}}\right] iT_2\Omega_p\rho_{gg}^{(0)}\Omega_B, \tag{16}$$

where $\rho_{ge}^{(B)}$ is the part of ρ_{ge} linear in the magnetic field, while $D_{p(d)} = \frac{\Gamma}{2} + i\delta_{p(d)}$ and $D_{pd} = \frac{3}{2}\frac{1}{T_2} + i\delta_R$ with $\delta_R = \delta_p - \delta_d$ being the Raman detuning. The steady state populations (14) were arrived at in the absence of the probe laser. These populations were then used in the full equations and were considered to be unaffected by the weak probe laser. The solution of the latter leads to the coherences (15), which reduce to the usual two-level atom equations for $\Omega_d = 0$, as should be the case. The rotation angle of the probe laser polarization is then given by [13]:

$$\phi = \frac{3}{8\pi}N\frac{\lambda^2}{A}\frac{\Gamma}{\Omega_p}[\Re(\rho_{\bar{g}e}) - \Re(\rho_{g\bar{e}})], \tag{17}$$

where $\Re(\rho_{xy})$ is the real part of ρ_{xy}. The solution for $\rho_{\bar{g}e}$ and ϕ is plotted in Fig. 3. It is to be noted that even narrower Raman resonances are readily observable [14]. The thick lines in the same figure come from a numerical simulation involving the full ^{85}Rb level structure, with the $5S_{1/2}$, $F = 3$ states corresponding to the $|g\rangle$ states, the $5S_{1/2}$, $F = 2$ corresponding to the $|c\rangle$ states, and the $5P_{1/2}$, $F = 2, 3$ corresponding to the $|e\rangle$ states. We concluded that the toy 6-level model gives an adequate qualitative description of the system dynamics and results in the same enhancement factor derived from the full numerical calculation. Thus the analytical expressions obtained for the 6-level system were integrated over a Maxwell velocity distribution in order to study the influence of the Doppler broadening on the magnetometer's operation. This was done by including the velocity dependence of the probe and drive laser detunings, $\Delta_{p(d)}(v) = \delta_{p(d)} - k_{p(d)}v$, with $k_{p(d)} = 2\pi/\lambda_{p(d)}$ and v the $\hat{\mathbf{x}}$-axis projection of the atomic velocity. The above calculations were performed for rubidium atoms, and we considered T_2 being determined by spin-destruction collisions, i.e., $1/T_2 = \sigma_{\mathrm{sd}}\bar{v}[\mathrm{Rb}] \approx 100$ Hz, where $\sigma_{\mathrm{sd}} = 9 \times 10^{-18}$ cm^2 [15] and [Rb] a typical rubidium number density. In the Doppler-free case, the optical pumping rate was $R \simeq 1/T_2$, while the Rabi frequency and detuning of the drive laser were $\Omega_d \simeq 5\sqrt{\Gamma/T_2}$ and $\delta_d = 4\Gamma$, respectively, and the Rabi frequency of the probe beam was $\Omega_p \simeq 3.3 \times 10^{-4}\Gamma = \text{const}$. After including Doppler broadening, Ω_p and R were left unchanged, whereas a numerical optimization procedure was followed to determine the optimum values for Ω_d and δ_d for any given value of atomic number density, resulting to $\delta_d \sim 200\Gamma$ and $\Omega_d \sim \Gamma$. In Fig. 4 we plot the rotation angle enhancement factor, β_ϕ, as a function of atom number

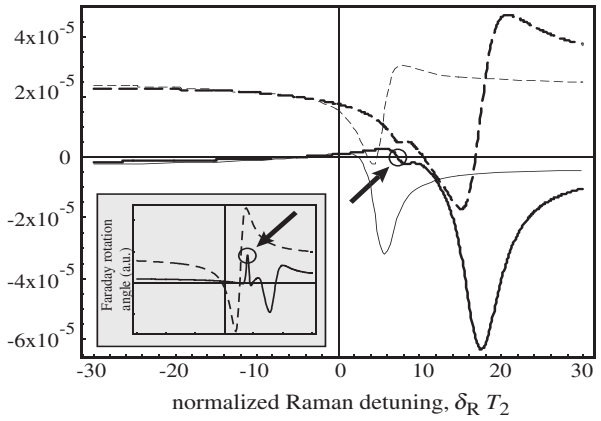

FIG. 3. Absorption (solid lines) and dispersion (dashed lines) profiles of the probe beam for the full ^{85}Rb structure (thick lines) and the toy 6-level model (thin lines). Inset: Faraday rotation angle for the full (solid line) and toy model (dashed line). The optimum point of operation is indicated by the arrows. The width of the Raman resonance is a few times $1/T_2 \approx 300$ Hz. The calculation was done for a magnetic field $B_y = 1$ fT, and for an alkali density $[\mathrm{Rb}] = 5 \times 10^{14}$ cm^{-3}. The profiles of the numerical calculation involving the full level structure of ^{85}Rb broaden and shift to the right due to higher Ω_d.

density. It can be seen that β_ϕ is lower when including Doppler broadening due to lowering and widening of the dispersion profiles, while their TLA counterparts are essentially unaffected (due to very large detunings). Moreover, for relatively low number densities there is no enhancement since the large Ω_d needed to create EIT conditions also requires large pumping rates for a point of zero absorption to appear, which leads to a reduction of the Faraday rotation angle and β_ϕ. However, we see that there is a useful range of atomic densities, spanning almost

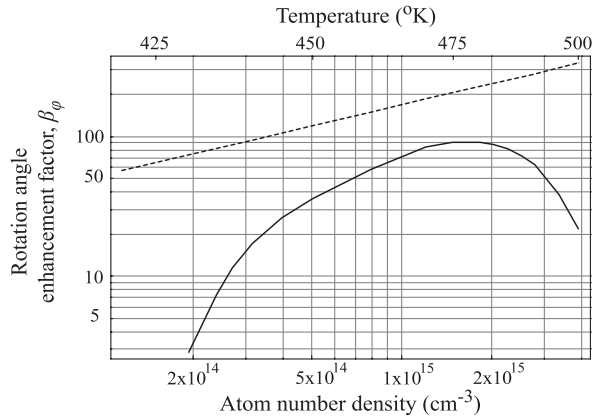

FIG. 4. Enhancement factor β_ϕ due to enhanced Faraday rotation of the probe laser polarization. Dashed line: Doppler-free case (both toy and full model); solid line: inclusion of Doppler broadening.

an order of magnitude, where enhancement is significant and can be used to expand the magnetometer's bandwidth.

In this Letter we have not treated the effects of the presence of a buffer gas on the EIT resonance, since there are several magnetometry applications using antirelaxation coated cells with no buffer gas [1,16]. Nevertheless, there is recent experimental evidence [17] concerning the high visibility of CPT resonances in alkali vapors with high buffer gas pressures. In conclusion, we have shown how to operate an atomic optical pumping magnetometer at frequencies almost 2 orders of magnitude higher than its bandwidth and still maintain a high signal-to-noise ratio. This measurement scheme could also be of use in quantum nondemolition techniques [18], where the absorption of probe laser photons prevents the realization of Heisenberg-limited magnetometry. Finally, even larger enhancements could be contemplated by entering into the gain region of the EIT resonance.

G. K. and I. K. K. wish to acknowledge support by Marie Curie Grant No. MIRG-CT-2004-004652.

*Electronic address: ikominis@iesl.forth.gr

[1] D. Budker, D. F. Kimball, S. M. Rochester, V. V. Yashchuk, and M. Zolotorev, Phys. Rev. A **62**, 043403 (2000).
[2] E. B. Aleksandrov *et al.*, Opt. Spektrosk. **78**, 325 (1995).
[3] M. Stähler, S. Knappe, C. Affolderbach, W. Kemp, and R. Wynands, Europhys. Lett. **54**, 323 (2001).
[4] H. Weinstock, *SQUID Sensors: Fundamentals, Fabrication and Applications* (Kluwer Academic, Dordrecht, 1996).
[5] J. C. Allred, R. N. Lyman, T. W. Kornack, and M. V. Romalis, Phys. Rev. Lett. **89**, 130801 (2002).
[6] I. K. Kominis, J. C. Allred, T. W. Kornack, and M. V. Romalis, Nature (London) **422**, 596 (2003).
[7] A. Draguhn, R. D. Traub, A. Bibbig, and D. Schmitz, J. Clin. Neurophysiol. **17**, 361 (2000).
[8] T. W. Kornack, R. K. Ghosh, and M. V. Romalis, Phys. Rev. Lett. **95**, 230801 (2005).
[9] D. Budker *et al.*, Rev. Mod. Phys. **74**, 1153 (2002).
[10] D. J. Wineland, J. J. Bollinger, W. M. Itano, F. L. Moore, and D. J. Heinzen, Phys. Rev. A **46**, R6797 (1992).
[11] T. Varpula and T. Poutanen, J. Appl. Phys. **55**, 4015 (1984).
[12] A. S. Zibrov *et al.*, Phys. Rev. Lett. **76**, 3935 (1996).
[13] M. Fleischhauer *et al.*, Phys. Rev. A **46**, 1468 (1992).
[14] S. Brandt, A. Nagel, R. Wynands, and D. Meschede, Phys. Rev. A **56**, R1063 (1997).
[15] A. B.-A. Baranga *et al.*, Phys. Rev. Lett. **80**, 2801 (1998).
[16] D. Budker, V. Yashchuk, and M. Zolotorev, Phys. Rev. Lett. **81**, 5788 (1998).
[17] A. B. Post, Y.-Y. Jau, N. N. Kuzma, and W. Happer, Phys. Rev. A **72**, 033417 (2005).
[18] M. Auzinsh *et al.*, Phys. Rev. Lett. **93**, 173002 (2004).